Europe are due to widespread soluble rocks, especially limestones. The very high loads of the Irrawaddy River in Southeast Asia and on New Guinea are produced by a combination of readily weathered rocks, high rates of weathering due to high temperatures and precipitation, and high discharges. The presence of crystalline rocks with low solubilities in much of Africa and Australia gives rise to generally low dissolved loads on those continents.

2.2.7.2 Particulate Material

The natural rate of erosion of particulate material is determined by climate, rock type, topography, tectonic activity, and vegetation. Wilkinson (2005) calculated that the current rate of movement of earth materials by humans (principally through agriculture, mining, forest clearing, and construction) is now more than 10 times the natural geologic rate of 7.2×10^9 T/yr (about 0.02 mm/yr). Thus these activities have greatly increased global sediment transport in historic times and, along with the effects of lakes and reservoirs acting as sediment traps (also greatly increased by humans; see Vörösmarty et al. 1997 and Graf 1999), strongly affect the global patterns of particulate-sediment yield.

Milliman and Syvitski (1992) found that contemporary particulate-sediment yields range from 1.2 to 36,000 T/km^2 · yr and are positively related to drainage area, maximum watershed elevation, and runoff (figure 2.35). The highest yields are in areas with seasonal-rainfall climates (compare figure 2.25) coupled with active mountain building (India) or highly erodible soils (China); high yields are also associated with mountain belts in Alaska, the Andes, and the western Mediterranean region, and in Taiwan, the Philippines, and New Zealand, where human activity also plays a significant role in sediment production. The areas of lowest yields (outside of deserts) are in northern North America and Eurasia, equatorial Africa, and eastern Australia, where low relief is coupled with resistant rocks and/or extensive vegetative cover.

2.2.7.3 Total Material Transport to Oceans

Table 2.11 shows estimates of dissolved and particulate-sediment loads and yields for the continents; the total load of dissolved plus particulate material to the oceans is about 17.4×10^9 T/yr. When allowance is made for the amount of sediment being trapped in reservoirs, the total rate of sediment transport is between 19.0×10^9 and 20.0×10^9 T/yr, of which about 80% is particulate and 20% is dissolved (Walling and Webb 1987). Assuming an average rock density of 2,500 kg/m^3, this total sediment yield represents the removal of 7.8×10^9 m^3/yr, or about 0.06 mm/yr worldwide. This is about twice the average erosion rate through geologic history (Wilkinson 2005).

Oceania and the Pacific Islands have the highest particulate and total yields due to their steep terrain and high precipitation. Europe has the highest dissolved yield and is the only continent in which dissolved load exceeds particulate load. Africa has the lowest particulate, dissolved, and total sediment yields due to its generally low relief, widespread resistant rocks, and extensive desert areas.

2.2.8 Climate Change and the Hydrologic Cycle

2.2.8.1 Overview

The atmospheric concentration of CO_2 (abbreviated as [CO_2]) before the industrial age was about 250 ppmv. The present concentration is about 400 ppmv, and figure 2.6 shows that global average temperature has increased by about 1°C since 1880 (Hansen et al. 2010). [CO_2] is expected to reach close to 1,000 ppmv by the end of the century if stringent efforts to reduce emissions are not implemented, and current climate models predict that this will increase global average temperature by 5 to 10°C. Figure 2.36 on p. 86 shows the global temperature forecast to 2030, accounting for the effects of solar variability, ENSO, volcanic activity, and anthropogenic causes (chiefly GHG emissions) using a model that was highly successful in reproducing temperature changes from 1980 to 2010. This model indicates that the **climate feedback factor** for CO_2 is about 0.5 to 1°C/(W/m^2). However, recent studies of [CO_2] through geological history indicate that the last time [CO_2] = 1,000 ppmv was 30 million years ago, when the average global temperature was about 16°C higher than today (~31°C). These reconstructions of the earth's actual climatic history suggest that the long-term feedback factor, which could include releases of methane from marine sediments and changes in vegetation and geological weathering rates, is closer to 2°C/(W/m^2). Thus, as noted by Kiehl (2011, p. 159),

> If the world reaches such concentrations of atmospheric CO_2, positive feedback processes can amplify global warming beyond current modeling estimates. The human species and global ecosystems will be placed in a climatic state never before experienced in their evolutionary history and at an unprecedented rate.

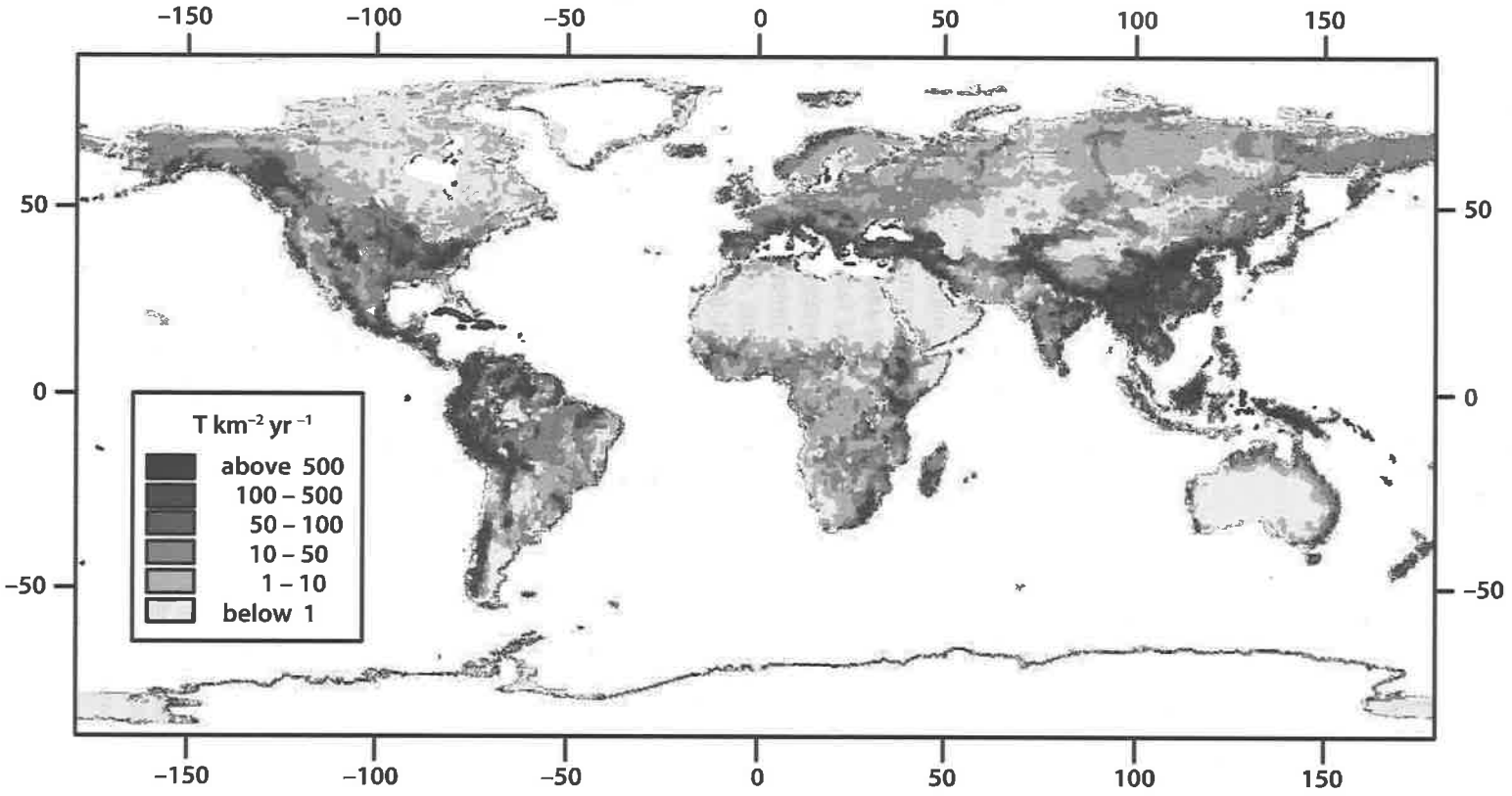

Figure 2.35 Global distribution of particulate-sediment yields. The highest rates are in the mountainous areas of Central and South America, the Alps and Caucasus, the Himalayas, and in central China. The lowest are in regions of low precipitation in the North American Arctic, and the deserts of north Africa and Australia [Ludwig and Probst (1998). River sediment discharge to the oceans: Present-day controls and global budgets. *American Journal of Science* 298:265–295, used with permission of *American Journal of Science*].

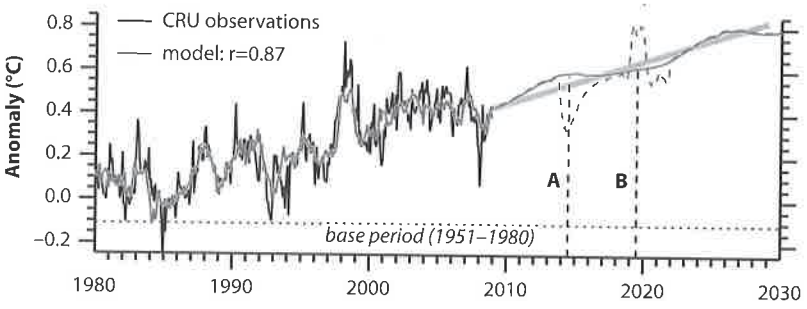

Figure 2.36 Observed global mean monthly temperatures (up to 2008) and forecast temperatures to 2030 incorporating effects of ENSO, volcanism, solar irradiance, and anthropogenic effects [Lean and Rind (2009)]. How will Earth's surface temperature change in future decades? *Geophysical Research Letters* 36, with permission of the American Geophysical Union].

The global hydrologic cycle is a major part of the earth's climate system, and will change in response to natural or anthropogenic climate changes. Much of the recent warming of the earth's surface is reflected in a rise in ocean temperatures (Murphy et al. 2009; Johnson et al. 2010), which causes an increase in evaporation. Both climate models and observations indicate that total atmospheric water vapor increases by about 7%/°C due to warmer air being able to hold more water vapor (Wentz et al. 2007), as dictated by the **Clausius–Clapeyron (C-C) relation** (box 2.2). Because warmer oceans and land surfaces will increase evaporation rates, and a warmer atmosphere can hold more water vapor, it is widely predicted that increasing temperature will cause an increase in global precipitation rates and an intensification of the hydrologic cycle. Satellite observations over the last two decades generally confirm this prediction; they indicate that global evaporation, total atmospheric water (more than 99% of which is in vapor form), total precipitation, and the intensities of the heaviest rainfall events have increased at about the rate predicted by the C-C relation (Allen and Ingram 2002; Wentz et al. 2007; Min et al. 2011; Durack et al. 2012). Theory also suggests that, because more rainfall is concentrated in larger storms, less will occur in smaller events and dry periods and droughts will last longer.

As shown in figure 2.37, current climate models do reasonably well at forecasting global precipitation, but recent precipitation changes have not simply followed global temperature. This is because precipitation changes are dominated by natural solar and volcanic forcing, which varies on short timescales, whereas the temperature response is dominated by steadily increasing anthropogenic GHG forcing.

Thus, past and future global warming will be accompanied by changes in the timing, amounts, and distributions of precipitation, evapotranspiration, snow, soil moisture, streamflow, and other factors; these in turn will force major adjustments in the magnitudes, timing, and locations of floods, droughts, water demands, supplies, and water quality. While complete examination of the likely hydrologic and water-resources impacts of these climate changes would require a separate book-length treatment, the next section provides a review of recent observed hydrologic changes and forecasts. Following this, section 2.2.8.3 explores the sensitivity of runoff to climate changes.

Box 2.2 Water-Vapor Capacity of the Atmosphere

The water-holding capacity of the air is given by the **saturation vapor pressure**, denoted e^*. The value of e^* depends on temperature, and its rate of change with temperature is given by the Clausius–Clapeyron equation, which is derived from thermodynamic principles (see, e.g., Peixoto and Oort 1992). In integrated form, the e^* versus temperature relationship is closely approximated as

$$e^* = 611 \cdot \exp\left(\frac{17.27 \cdot T}{T + 237.3}\right), \qquad \textbf{(2B2.1)}$$

where e^* is in pascals (= N/m^2) and T is temperature in °C. Thus e^* increases approximately exponentially with temperature (figure 3.3); at earth-surface temperatures, this rate is about 6.5%/°C to 7%/°C.

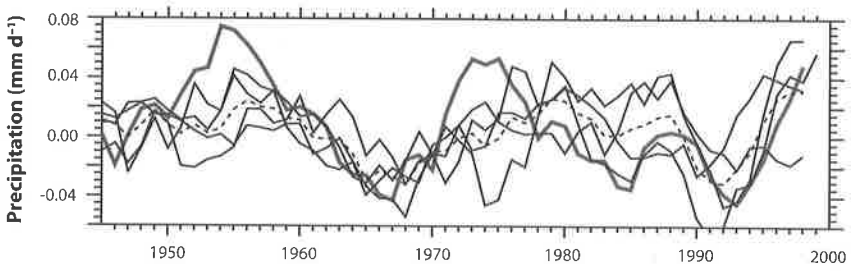

Figure 2.37 Variability of global mean precipitation, 1945–2000. Darkest line shows measured values, other solid lines are model estimates. The dashed line is an average of the models [Allen and Ingram (2002). Constraints on future changes in climate and the hydrologic cycle. *Nature* 419:224–232. Reprinted by permission from Macmillan Publishers Ltd.].

2.2.8.2 Evidence for Recent Climate-Related Hydrologic Changes

Huntington (2006) reviewed recent evidence for the intensification of the global hydrologic cycle that is predicted to accompany global warming; his results are summarized below and in table 2.12. Additional reports of recent climate-related hydrologic changes are noted in box 2.3.

Huntington (2006) reported evidence that global land precipitation increased by about 2% over the twentieth century, but with significant regional variations: Land precipitation increased by 7 to 12% between 30 and 85°N and by 2% between 0 and 55°S, but with substantial decreases in some regions. In the United States, spring, summer, and fall precipitation increased during the twentieth century, but there was little change in Canada.

Increases in snow-water equivalent averaging about 4 to 5% per decade were reported in North America and Russia. There was variability in the extent of seasonal snow cover in fall and winter, but there were widespread decreases in spring snow-cover extent across Russia, China, and the Swiss Alps, and the extent of spring snow cover decreased rapidly after 1980 in North America. The ratio of snow to total precipitation decreased in March in New England in the United States and in Canada south of 55°N latitude.

A number of hydrologic and phenological studies cited by Huntington (2006) showed that the length of the growing season has increased substantially, suggesting that evapotranspiration has increased, at least in humid regions. Evapotranspiration increases of about 1 mm/yr have also been inferred from hydrologic budget analyses of four major US river basins from 1950 to 2000. Other studies found increases in lower troposphere water vapor (precipitable water content) in the last half of the twentieth century. Although cloudiness increased before the 1980s, the trend reversed during the late 1980s to the early 1990s, so the long-term trend remains uncertain. The diurnal temperature range, which is inversely related

Table 2.12 Summary of Trends in Land-Area Hydroclimatic Variables.

Variable	Twentieth Century	Latter Half of the Twentieth Century
Precipitation	Increasing (R, G)	
Runoff	Increasing (R, G)	Increasing (R, G)
Tropospheric water vapor		Increasing (R)
Cloudiness		No change
Tropical storm frequency and intensity		No change
Floods	No change	Increasing (R, G)
Droughts		Increasing (R)
Soil moisture		Increasing (R)
Seasonal glacier mass balance		Increasing (G)
Pan evaporation		Decreasing (R)
Actual evapotranspiration		Increasing (R)
Growing-season length[a]	Increasing (R)	Increasing (R)
Growing-season length[b]		Increasing (R)

R = regional
G = global
[a]Based on records of temperature or agricultural killing frost.
[b]Based on satellite-derived "onset of greenness" normalized difference vegetation index.

Source: Huntington (2006).

Box 2.3 A Sampling of Reports of Recent Large-Scale Changes in the Hydrologic Cycle[a]

Cloud Cover, Humidity, and Wind Speed

- Atmospheric water content (precipitable water) has increased globally since about 1988 (Wentz et al. 2007).
- Atmospheric water vapor has increased at a rate of 0.27 mm per decade from 1988 to 2006; the increase is largest in the tropics and Northern Hemisphere and relatively small in the Southern Hemisphere (Mears et al. 2010).
- Water vapor over the oceans increased by 2.4% from 1988–2006 (Wentz et al. 2007).
- Wind speeds over the global ocean have increased by 5 to 10% over the last 20 years (Young et al. 2011).
- Cloud cover increased over wide areas of the globe since 1900 (Henderson-Sellers 1992; Karl et al. 1993; Dai et al. 1997).

Precipitation

- Global precipitation increased by 2.8% from 1988–2006 (Wentz et al. 2007).
- Global land precipitation has increased by about 30 mm/yr since 1900 (Levinson et al. 2010).
- Precipitation in the Arctic has generally increased in the last century, especially in winter (Hinzman et al. 2005).
- The number of land-falling tropical cyclones in the United States has increased since 1994, and the number of heavy rainfall events associated with those storms was more than double the long-term (1895–2008) average (Kunkel et al. 2010).
- From 1970 to 2004 the number of category 4 and 5 hurricanes has increased globally; this increase is directly linked to increasing sea-surface temperatures (Hoyos et al. 2005).
- In the midlatitudes, there is a widespread increase in the frequency of very heavy precipitation during the past 50 to 100 years (Groisman et al. 2005).
- Precipitation increased in southern Canada by 13%, in northern Canada by 20%, and in the United States by 4% during the last 100 years; greatest increases were in eastern Canada and adjacent regions of the United States (Groisman and Easterling 1994).
- Decadal to multidecadal variability of global precipitation increased since 1900 (Tsonis 1996).
- Proportion of precipitation occurring in extreme one-day events increased in the United States in the last 30 to 80 years (Karl et al. 1995).
- Fall precipitation increased in central United States between 1948 and 1988 (Lettenmaier et al. 1994).
- The 2010 drought in the Amazon rain forest was unique in timing and intensity since record keeping began (1903). Since the mid-1970s, the length of the dry season and the number of "dry" and "very dry" events have increased (Marengo et al. 2011).

Snow

- Snowpack reductions in the northern US Rocky Mountains in the last 50 years are almost unprecedented compared to the previous 800 years, and are due to springtime warming caused by positive reinforcement of anthropogenic warming by decadal variability (Pederson et al. 2011).
- The average annual duration of Northern Hemisphere snow cover has decreased by 15 to 18 days since the early 1970s (Dye 2002).
- A rapid reduction in arctic snow-cover duration (due primarily to an early disappearance of snow cover in spring) occurred in the 1980s and has continued (Dirksen et al. 2010).
- Snow-covered areas have declined in all latitude bands in the Northern Hemisphere since 1973 (Pielke et al. 2004).
- Spring snow-cover extent in the Northern Hemisphere declined steadily and decreased by about 8% from the 1970s to 2000s (Robinson 2010).
- Areal snow cover in the Northern Hemisphere declined 10% in the past 20 years (Groisman et al. 1994).
- Northern Hemisphere snow-cover extent decreased by 2.5 to 5% between 1978 and 1999 (Comiso and Parkinson 2004).

Evapotranspiration

- Pan evaporation in the United States and former Soviet Union has declined since 1950 (Peterson et al. 1995).
- Pan evaporation in China decreased by 5.4 mm/yr^2 from 1960 to 1991 due to decreasing wind speed and insolation offsetting increased temperature, then increased by 7.9 mm/yr^2 from 1992 to 2007 as the temperature effect became dominant (Liu et al. 2011).
- Global atmospheric evaporative demand has declined over the last 50 years, largely due to a 0.7 m/s decline in wind speed (McVicar et al. 2012).
- Global evaporation increased by 2.6% from 1988–2006 (Wentz et al. 2007).

Streamflow

- Streamflow remained steady or increased over the last decade (2000–2009) in all continents and ocean catch-

ments, except Africa and the Mediterranean/Black Sea drainage, when compared to the long-term mean (Fekete et al. 2010).

- Annual streamflow increased by 15.5% over northern Canada from 1964–2007, consistent with other parts of the Arctic (Déry et al. 2009).
- Shrinking glaciers and snowpacks are reducing discharge in rivers that drain the central Rocky Mountain region (Wolfe et al. 2011).
- Mean annual discharge from the six largest rivers of the Eurasian Arctic increased about 12% from 1936 to 2009 (Shiklomanov 2010).
- Mean annual discharge from the four largest rivers of the North American Arctic increased about 10% from 1970 to 2009 (Shiklomanov 2010).
- Winter–spring streamflow strongly increased at over 50% of US gauging stations from 1948 to 1988, with strongest trends in north-central region (Lettenmaier et al. 1994).
- Streamflow has increased, especially in fall and winter, during past 50 years in most of conterminous United States (Lins and Michaels 1994).
- Runoff has increased in the United States between 1900 and 2008, and precipitation has accounted for almost all of the runoff variability during that period (McCabe and Wolock 2011).

Lakes

- The number and size of lakes on permafrost areas in Siberia have decreased by 11% and 6% respectively between 1973 and 1998, almost certainly due to permafrost melting (Smith et al. 2005).
- Surface water of large lakes around the world warmed by 0.045 to 0.10°C/yr from 1985 to 2009, with far greater warming in the mid- and high latitudes of the Northern Hemisphere than in low latitudes and the Southern Hemisphere (Schneider and Hook 2010).

Glaciers and Permafrost

- Most arctic glaciers experienced net loss of water since 1940, contributing 0.13 mm/yr to sea-level rise (Dowdeswell et al. 1998).
- Permafrost warmed by up to 4°C in Alaska since 1976 (Osterkamp 2007).
- Over the last 18 years, the rate of loss of ice from the earth's glaciers accelerated at the following rates: Greenland—21.9 Gt/yr^2, Antarctica—14.5 Gt/yr^2, mountain glaciers and ice caps—12.6 Gt/yr^2 (Rignot et al. 2011).
- The average balances for arctic glaciers have been generally negative over the past 40 years (Hinzman et al. 2005).
- There was an abrupt, large increase in the extent of permafrost degradation in northern Alaska since 1982 associated with record warm temperatures during 1989–1998, mainly in massive ice wedges that had been stable for thousands of years (Jorgenson et al. 2006).
- The rate of mass loss from four glaciers in the Canadian arctic islands was 5 to 7 times faster in 2005–2009 than in 1963–2004 (Sharp et al. 2011).
- Permafrost temperatures increased 0.5 to 2°C during the last several decades in Alaska, northwest Canada, Siberia, and northern Europe (Romanovsky et al. 2010).
- Alpine glacier mass balances were generally negative for the eighteenth consecutive year. Decadal mean annual mass balance was −198 mm in the 1980s, −382 mm in the 1990s, and −624 mm for 2000–2008 (Pelto 2010).
- The portion of the Greenland ice sheet experiencing summer melting expanded by 17% from 1992 to 2002 (Comiso and Parkinson 2004).

Growing Season and Plant Growth

- Plant growth in northern high latitudes increased from 1981 to 1991 (Myneni et al. 1997).
- Growing season has increased by 10 to 20 days in the last few decades, largely due to earlier beginning (Linderholm 2006).

[a]See also Loaiciga et al. (1996), Huntington (2006), Arndt (2010), Lubchenco and Karl (2012).

to cloudiness, decreased over most land areas in the latter half of the twentieth century.

Streamflow is a particularly meaningful indicator of climate change because (1) it areally and temporally integrates precipitation and evapotranspiration and (2) it amplifies changes in precipitation: Karl and Riebsame (1989) concluded that a given relative change in precipitation is amplified to a one- to sixfold change in relative streamflow (see discussion in section 2.2.8.3). However, streamflow is also directly affected by anthropogenic changes due to water imports and exports, reservoir construction, irrigation, etc.

Sources cited by Huntington (2006) indicated an increase in continental runoff generally during the twentieth century, from individual major rivers globally and from many smaller rivers in the Northern Hemisphere. This is consistent with the study of Labat et al. (2004), who found a 4% increase in global runoff for each 1°C temperature increase between 1875 and 1994 (figure 2.38). However, regional variations were significant: runoff increased in North America, Asia, and South America; decreased in Africa; and showed no trend in Europe. In contrast, Pekárová et al. (2003) found no significant trends in the streamflows of large rivers from all continents (except Antarctica) over the nineteenth and twentieth centuries, but identified cycles averaging 14 and 28 years, and a 20- to 22-year cycle in some regions. These cycles may be related to teleconnections (section 2.1.6), and may appear to be trends when shorter time periods are examined.

An important question is to what extent observed and forecast temperature changes affect the frequency and intensity of extreme weather events such as hurricanes, floods, and droughts. Huntington (2006) cited several regional studies that report increases in intense precipitation events, but found no definitive evidence of change in the intensity of tropical storms. However, Kunkel et al. (2010) reported that the number of land-falling tropical cyclones in the United States has increased since 1994, and the number of heavy rainfall events associated with those storms was more than double the long-term (1895–2008) average. A few studies found an increase in the frequency of extreme floods, but others did not detect trends in flooding in the United States, Canada, Scandinavia, or central Europe.

A global analysis by Dai et al. (2004) found that, since the 1970s, the fraction of land surface characterized as "very dry" more than doubled, while "very wet" areas declined slightly; another study (Robock et al. 2000) found increases in areas of both severe drought and moisture surplus. Huntington (2006) reported considerable evidence for lengthen-

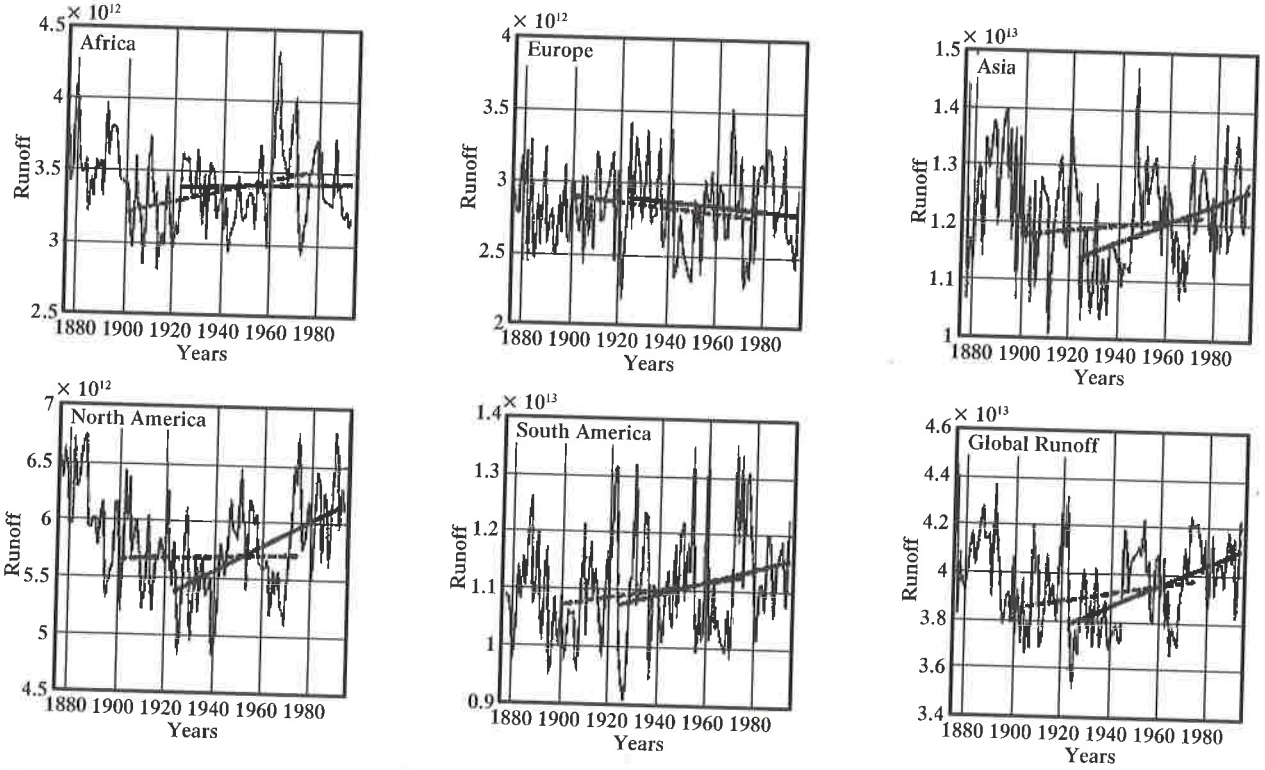

Figure 2.38 Mean annual runoff (in L/s) for five continents and linear trends for 1900–1970 and 1925–1994 intervals. Except for the African and European continents, mean annual runoff increases more rapidly during the second period, coincident with a rapid global warming [Labat et al. (2004). Evidence for global runoff increase related to climate warming. *Advances in Water Resources* 27:631–642, with permission of Elsevier].

ing of the growing season throughout the Northern Hemisphere which, along with increasing temperatures, would be expected to be associated with increased evapotranspiration and decreased growing-season soil moisture. Robock et al. (2000) reported increases in summer soil moisture in recent decades at almost all sites having long-term records; they attributed this to increases in precipitation and cloud cover that more than compensated for increased evapotranspiration. Temperature increases over the last century appear to have increased the frequency of ENSO events, and these regionally variable changes in dryness and wetness are attributed to both ENSO-induced decreases in precipitation and warming-induced increases in evaporation.

Huntington's (2006) review found that subpolar and mountain glaciers throughout the world are losing mass in response to warming. One study found that many such glaciers are experiencing higher winter snowfall that is more than compensated by increased summer ablation, which is further evidence for a recent intensification of the hydrologic cycle. There is consistent evidence of later freeze-up and earlier break-up in rivers and lakes in the Northern Hemisphere from 1846 to 1995; over this period freeze-up dates averaged 5.8 days per 100 years later, and break-up dates averaged 6.5 days per 100 years earlier. A few longer time series reveal reduced ice cover beginning as early as the sixteenth century, with increasing rates of change after about 1850. Earlier spring snowmelt runoff was reported in Siberia and western United States and Canada, earlier river and lake ice-out in New England, and a longer frost-free season in the United States between 1948 and 1999.

Huntington (2006) concluded that the widespread increases in precipitation, evapotranspiration, water vapor, and runoff noted above suggest that the theoretically expected intensification of the water cycle has occurred during at least the last half of the twentieth century, and more recent studies (box 2.3) suggest that this trend is continuing. Observations of ocean salinity showing a 3% decrease in precipitation minus evaporation in subtropical oceans (a relative increase in evaporation) and 7% (Northern Hemisphere) and 16% (Southern Hemisphere) increases in high-latitude oceans (a relative increase in precipitation) reinforce this conclusion (Helm et al. 2010).

2.2.8.3 Runoff Sensitivity to Climate Change

Because runoff spatially and temporally integrates hydrologic inputs and outputs, and because long-term average runoff represents the available water resource of a region (section 1.8.1), the sensitivity of runoff to climate change is a critical concern. Here we explore this question using simple analytical relations among long-term average water- and energy-balance quantities (expressed as water fluxes [L T^{-1}]). To make the notation less cumbersome here we use simpler symbols to represent the water-balance components introduced in section 1.8: $P \equiv \mu_P$, $ET \equiv \mu_{ET}$, $RO \equiv \mu_{RO}$.

These relations begin with an expression relating evapotranspiration, *ET*, to precipitation, *P*, and potential evapotranspiration, *PET*, which expresses the evaporative demand of the climate (section 2.2.3):

$$ET = f_B(P, PET). \tag{2.9}$$

The function f_B is a "Budyko-type equation," named for the Russian climatologist M. I. Budyko, who explored such relations (Budyko 1958, 1974). Although many versions of f_B have been proposed, Yang et al. (2008) used physical, dimensional, and mathematical reasoning to show that the appropriate form of a simple relation between *ET* and climate is

$$ET = \frac{PET \cdot P}{(P^w + PET^w)^{1/w}}, \; w > 0, \tag{2.10}$$

where w is a parameter that depends on watershed characteristics. Because of interrelations among these characteristics, it is difficult to specify a physically based relation for w. However, Yang et al. (2007) established empirical relations for nonhumid regions of China, indicating that w (1) increases with the ratio of soil hydraulic conductivity to rainfall rate and the ratio of soil-water storage capacity to potential evapotranspiration and (2) decreases with average watershed slope.

Figure 2.39 shows the relation between *ET*/*P* and *PET*/*P* as given by equation (2.10). The ratio *PET*/*P* is called the **aridity index**; actual evapotranspiration is **energy-limited** in humid regions (*PET*/*P* < 1) and **water-limited** in arid regions (*PET*/*P* > 1). Curves with low values of w characterize regions with relatively small storage (e.g., rocky, steeply sloping watersheds where rainfall is quickly converted to runoff), while those with high w values represent relatively flat watersheds with high subsurface storage.

From section 1.8, average precipitation, *P*, evapotranspiration, *ET*, and runoff, *RO*, are related as

$$RO = P - ET, \tag{2.11}$$

where we assume no long-term storage changes or ground-water inputs. Combining (2.10) and (2.11) gives a relation between runoff and climate:

$$RO = P \cdot \left[1 - \frac{PET}{\left(P^w + PET^w \right)^{1/w}} \right]. \quad \textbf{(2.12)}$$

We can now use equation (2.12) to explore how *RO* responds to climate changes, i.e., changes in *PET* and *P*. Taking derivatives of (2.12) yields

$$\frac{\partial RO}{\partial P} = 1 - \frac{1}{\left[1 + \left(\frac{P}{PET} \right)^w \right]^{1+1/w}} \quad \textbf{(2.13)}$$

and

$$\frac{\partial RO}{\partial PET} = -\frac{1}{\left[1 + \left(\frac{PET}{P} \right)^w \right]^{1+1/w}}. \quad \textbf{(2.14)}$$

Note that (2.13) and (2.14) assume that precipitation and potential evapotranspiration are independent. We have seen in section 2.2.3 and box 2.2 that both *P* and *PET* are positively related to temperature at the global scale, but the relations vary regionally, even in sign, so it is reasonable as a first approximation to assume independence at the watershed scale. [See Yang et al. (2008) for further discussion.]

Equations (2.13) and (2.14) are graphed in figure 2.40. Figure 2.40a shows that, in humid regions ($PET/P < 1$), most of a change in precipitation is reflected in a change in runoff ($\partial RO/\partial P > 0.5$), with little effect due to watershed characteristics. In arid regions ($PET/P > 1$), the effect of a precipitation change on runoff varies strongly with watershed type, being small in watersheds with large storage (large *w*) and much greater where storage is small. Figure 2.40b shows that watershed type has a much greater effect on $\partial RO/\partial PET$ in humid regions than in arid regions.

The sensitivity of runoff to changes in climate is usually expressed as **climate elasticity**, defined as the ratio of the relative change in runoff, dRO/RO, to the relative change in the climatic parameters. Thus the elasticity of runoff to precipitation, $\varepsilon(RO,P)$, is

$$\varepsilon(RO,P) \equiv \frac{dRO/RO}{dP/P} = \frac{dRO \cdot P}{dP \cdot RO}. \quad \textbf{(2.15)}$$

This expression is evaluated in box 2.4 on p. 94 and graphed in figure 2.41 on p. 95. Note that all values of $\varepsilon(RO,P)$ are greater than 1, indicating that a 1% increase in precipitation produces a greater than 1% increase in runoff. Elasticity increases with *w* and decreases with increasing precipitation.

As noted in box 2.4, it is more meaningful to related fractional changes in runoff to absolute, rather than relative, increments of temperature, so that we express the temperature elasticity of runoff as

$$\varepsilon(RO,T) \equiv \frac{dRO/RO}{dT} = \frac{dRO}{RO \cdot dT}. \quad \textbf{(2.16)}$$

Using an expression relating *PET* to temperature [equation (2B4.2); figure 2.42 on p. 96], the expression for this is derived in box 2.4 and plotted in figure 2.43 on p. 97. As expected, $\varepsilon(RO,T)$ values are negative; they are also much smaller than $\varepsilon(RO,P)$ values.

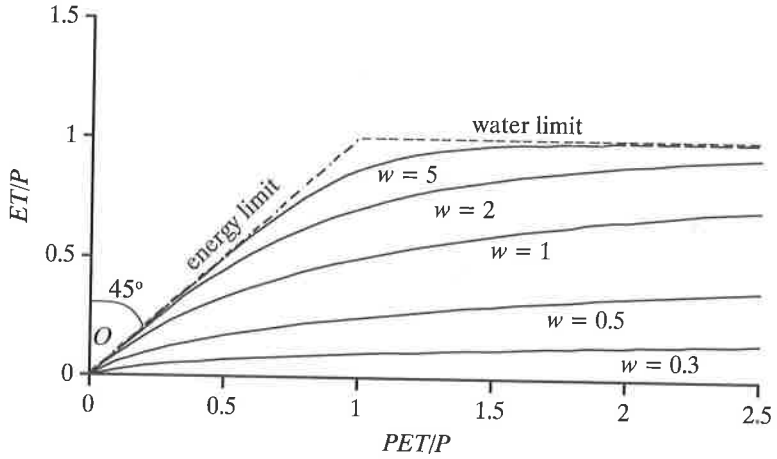

Figure 2.39 The relation between *ET/P* and *PET/P* as given by equation (2.10). The ratio *PET/P* (horizontal axis) is the aridity index; The parameter *w* characterizes regional water storage [Yang et al. (2008). New analytical derivation of the mean annual water-energy balance equation. *Water Resources Research* 44, with permission of the American Geophysical Union].

Some example calculations of elasticity/sensitivity using the above relations are given in box. 2.4.

The climate elasticity of runoff has also been investigated using more elaborate hydrologic models and empirically by examination of streamflow and climatic data. The conclusions of these studies are generally consistent with those determined via equation (2.12). For example, Karl and Riebsame (1989) examined the sensitivity of streamflow in the United States to changes in temperature and precipitation using historical data and concluded that 1 to 2°C temperature changes typically have little effect on streamflow, whereas a given relative change in precipitation produces a one- to sixfold change in streamflow. Sankarasubramanian et al. (2001) found empirical values of $\varepsilon(RO,P)$ ranging from 1 to 3.5 in the United States, with highest values in semiarid regions, and Sankarasubramanian and Vogel (2003)

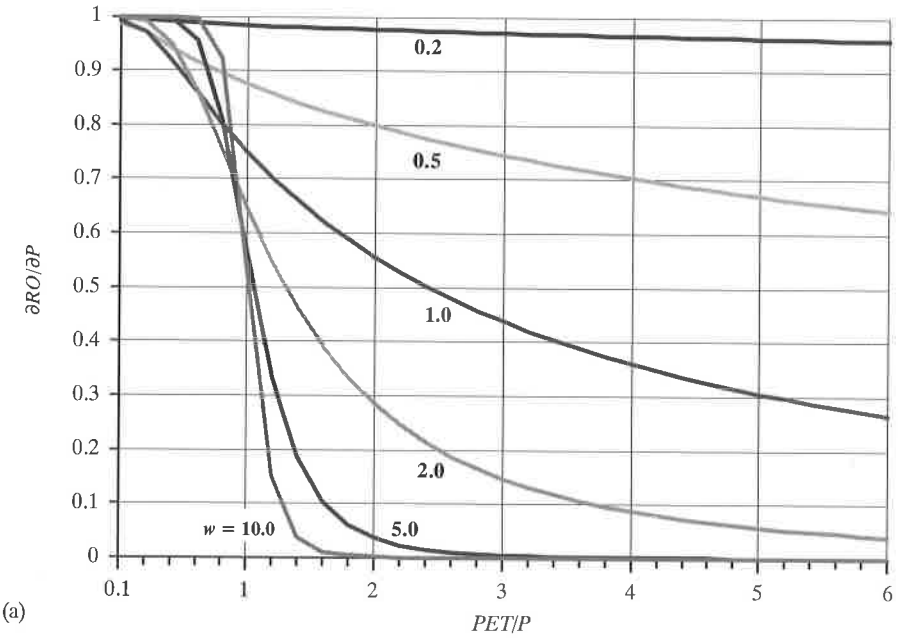

(a)

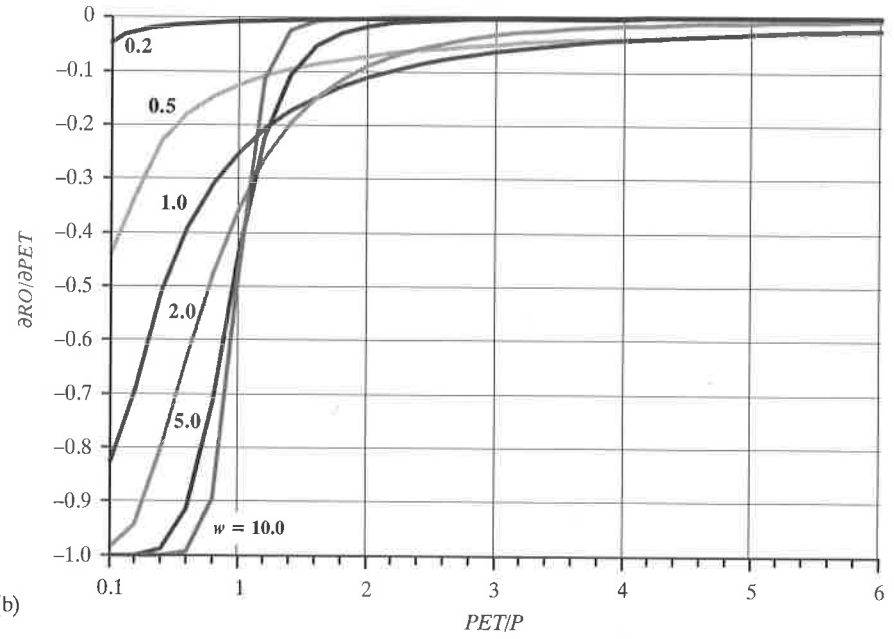

(b)

Figure 2.40 (a) $\partial RO/\partial P$ as a function of aridity index, PET/P [equation (2.13)]. (b) $\partial RO/\partial PET$ as a function of inverse of aridity index [equation (2.14)].

Box 2.4 Derivation of Runoff Elasticity to Changes in Precipitation and Temperature

Precipitation Elasticity

From (2.12) and (2.13) we can write the elasticity of runoff to precipitation, $\varepsilon(RO,P)$ as

$$\varepsilon(RO,P) \equiv \frac{dRO/RO}{dP/P} = \frac{1-\dfrac{1}{\left[1+\left(\dfrac{P}{PET}\right)^{w}\right]^{1+1/w}}}{1-\dfrac{PET}{\left(P^{w}+PET^{w}\right)^{1/w}}}. \qquad \textbf{(2B4.1)}$$

Temperature Elasticity

Given the strong dependence of potential evapotranspiration on temperature, a number of formulas have been used for estimating monthly average potential evapotranspiration from monthly average temperature alone (see section 6.7.2.1). For estimating *annual PET* from average annual air temperature, Gardner (2009) used

$$PET = 1.2\times10^{10}\cdot\exp(-4{,}620/\mathcal{T}), \qquad \textbf{(2B4.2)}$$

where PET is in mm/yr and $\mathcal{T}$ is mean annual air temperature (K). Although this relationship is approximate, we use it to explore the essential aspects of hydrologic response to climate change.

The change of runoff with temperature is found as

$$\frac{\partial RO}{\partial \mathcal{T}} = \frac{\partial RO}{\partial PET}\cdot\frac{\partial PET}{\partial \mathcal{T}}. \qquad \textbf{(2B4.3)}$$

From (2B4.2),

$$\frac{\partial PET}{\partial \mathcal{T}} = \frac{5.54\times10^{13}\cdot\exp\left(-4{,}620/\mathcal{T}\right)}{\mathcal{T}^{2}}. \qquad \textbf{(2B4.4)}$$

Substituting (2.12) and (2B4.4) into (2B4.3) then gives

$$\frac{\partial RO}{\partial \mathcal{T}} = -\frac{5.54\times10^{13}\cdot\exp\left(-4{,}620/\mathcal{T}\right)}{\left[1+\left(\dfrac{PET}{P}\right)^{w}\right]^{1+1/w}\cdot\mathcal{T}^{2}}. \qquad \textbf{(2B4.5)}$$

Equation (2B4.5) could be used to calculate the elasticity of runoff to temperature, $\varepsilon(RO,\mathcal{T})$, as

$$\varepsilon(RO,\mathcal{T}) \equiv \frac{\partial RO/RO}{\partial \mathcal{T}/\mathcal{T}}. \qquad \textbf{(2B4.6)}$$

However, because $\mathcal{T}$ is a large number, it is more meaningful to relate a fractional change in runoff to an actual temperature increment, $d\mathcal{T}$, rather than to a relative change $\partial\mathcal{T}/\mathcal{T}$. This relation is found by multiplying (2B4.5) by $d\mathcal{T}$ and dividing by (2.12):

$$\frac{\partial RO}{RO} = -\frac{5.54\times10^{13}\cdot\exp\left(-4{,}620/\mathcal{T}\right)}{\mathcal{T}^{2}\cdot P\cdot\left[1+\left(\dfrac{PET}{P}\right)^{w}\right]^{1+1/w}\cdot\left[1-\dfrac{PET}{\left(P^{w}+PET^{w}\right)^{1/w}}\right]}\cdot d\mathcal{T}, \qquad \textbf{(2B4.7)}$$

where PET is given by (2B4.2).

Example Calculations

Here we use the above relationships to compare the changes in average runoff resulting from a 7% increase in average precipitation and a 1°C increase in average temperature in watersheds with $w = 0.5$ and $w = 2$ in two regions:

Region	Annual P (mm)	Annual T (°C)
Humid temperate	1,000	10
Arid subtropical	200	20

Referring to the figures indicated, we find:

Table 2B4.1 Humid Temperate Region.

w	Figure	$\varepsilon(RO,P)$	Figure	$\partial RO/RO\cdot d\mathcal{T}$
0.5	2.41a	1.17	2.43a	−0.010
2	2.41c	2.19	2.43c	−0.069

Table 2B4.2 Arid Subtropical Region.

w	Figure	$\varepsilon(RO,P)$	Figure	$\partial RO/RO\cdot d\mathcal{T}$
0.5	2.41a	1.32	2.43a	−0.017
2	2.41c	2.98	2.43c	−0.106

Multiplying the above values by the increases in P and T gives the following values of dRO/RO:

Table 2B4.3 Humid Temperate Region.

w	Due to $dP/P = 0.07$	Due to $d\mathcal{T} = 1$°C
0.5	0.082	−0.010
2	0.153	−0.069

Table 2B4.4 Arid Subtropical Region.

w	Due to $dP/P = 0.07$	Due to $d\mathcal{T} = 1$°C
0.5	0.092	−0.017
2	0.209	−0.106

Thus the runoff responses are considerably larger (in absolute value) in the arid subtropical watersheds, and for a given climate, are considerably larger in watersheds with more storage.

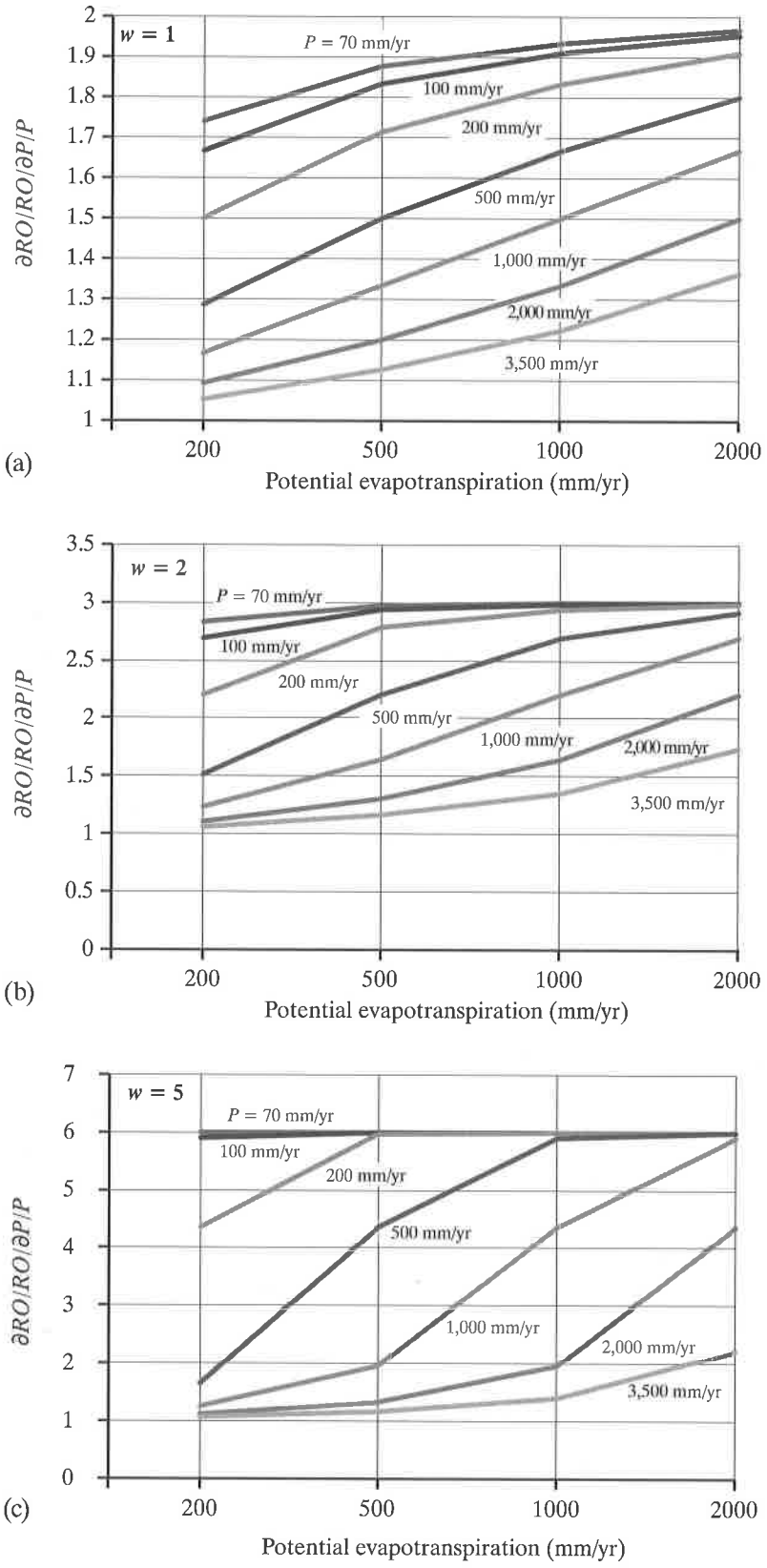

Figure 2.41 Elasticity of runoff to precipitation, $\varepsilon(RO,P)$, as a function of potential evapotranspiration, *PET*, and precipitation, *P* [equation (2B4.1)]. (a) $w = 1$; (b) $w = 2$; (c) $w = 5$.

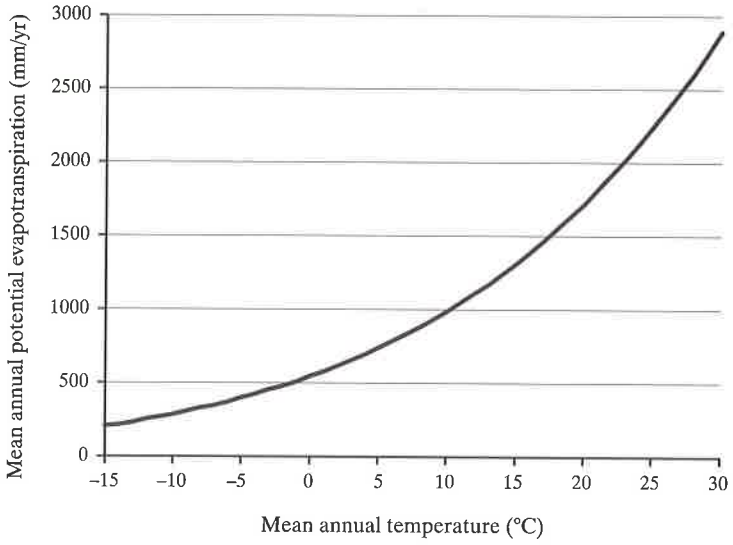

Figure 2.42 Generalized relation of average annual potential evapotranspiration as a function of mean annual temperature as postulated by Gardner (2009) [equation (2B4.2)].

showed that $\varepsilon(RO,P)$ values depend on the aridity index and soil-water storage. Yang and Yang (2011) found $\varepsilon(RO,P)$ ranging from 1.6 to 3.9 and $\varepsilon(RO,T)$ ranging from -0.02 to $-0.11°C^{-1}$ in two large Chinese watersheds. McCabe and Wolock (2011) reported that runoff has increased in the United States during the past century and that precipitation has accounted for almost all of the runoff variability, while temperature effects have been small, even though temperatures have increased significantly. Tang and Lettenmaier (2012) found that $\varepsilon(RO,P)$ ranges from 1 to 3 and $\varepsilon(RO,T)$ from 0.02 to $0.06°C^{-1}$ in major global watersheds.

The general conclusions from all of these studies are:

1. $\varepsilon(RO,P) > 1$ everywhere and typically ranges from 1 to 3 or more;
2. $\varepsilon(RO,P)$ increases with mean annual evapotranspiration and temperature and decreases with mean annual precipitation;
3. For a given climate, $\varepsilon(RO,P)$ increases with watershed storage (w);
4. In humid regions ($PET/P < 1$), a change in precipitation (dP) mostly transforms into runoff ($dRO > dET$).
5. In arid regions ($PET/P > 1$), a change in precipitation (dP) mostly transforms into evapotranspiration ($dRO < dET$).
6. $\varepsilon(RO,T)$ typically ranges from -0.02 to $-0.10°C^{-1}$; and
7. The effects of global warming-induced precipitation changes on runoff will be greater than the effects of increased evapotranspiration due to temperature increase.

The above conclusions appear to be well founded theoretically and supported by observation. However, predicting the magnitude, and even the direction, of local and regional hydrologic change due to climate and land-use change is challenging because many factors are involved in addition to the direct responses to changes in precipitation and temperatures. For example, experiments indicate that higher CO_2 concentrations tend to reduce water use by plants (Lemon 1983), and this could offset increases in evapotranspiration from land surfaces due to the temperature effect. Thus, one plausible scenario is that evaporation from the oceans will increase, while land evapotranspiration will change little, or perhaps even decrease. Further uncertainty exists because of the difficulty in predicting the hydrologic effects of changes in length of growing season, area of plant cover, plant species, wind speed, and cloudiness, and because there is considerable feedback between land evapotranspiration and global temperature and precipitation (Shukla and Mintz 1982; Loaiciga et al. 1996).

2.2.8.4 Moisture Recycling

A major aspect of this feedback is the recycling of continental precipitation and evapotranspiration. To study these phenomena globally, van der Ent et al. (2010) split the total precipitation at a given point

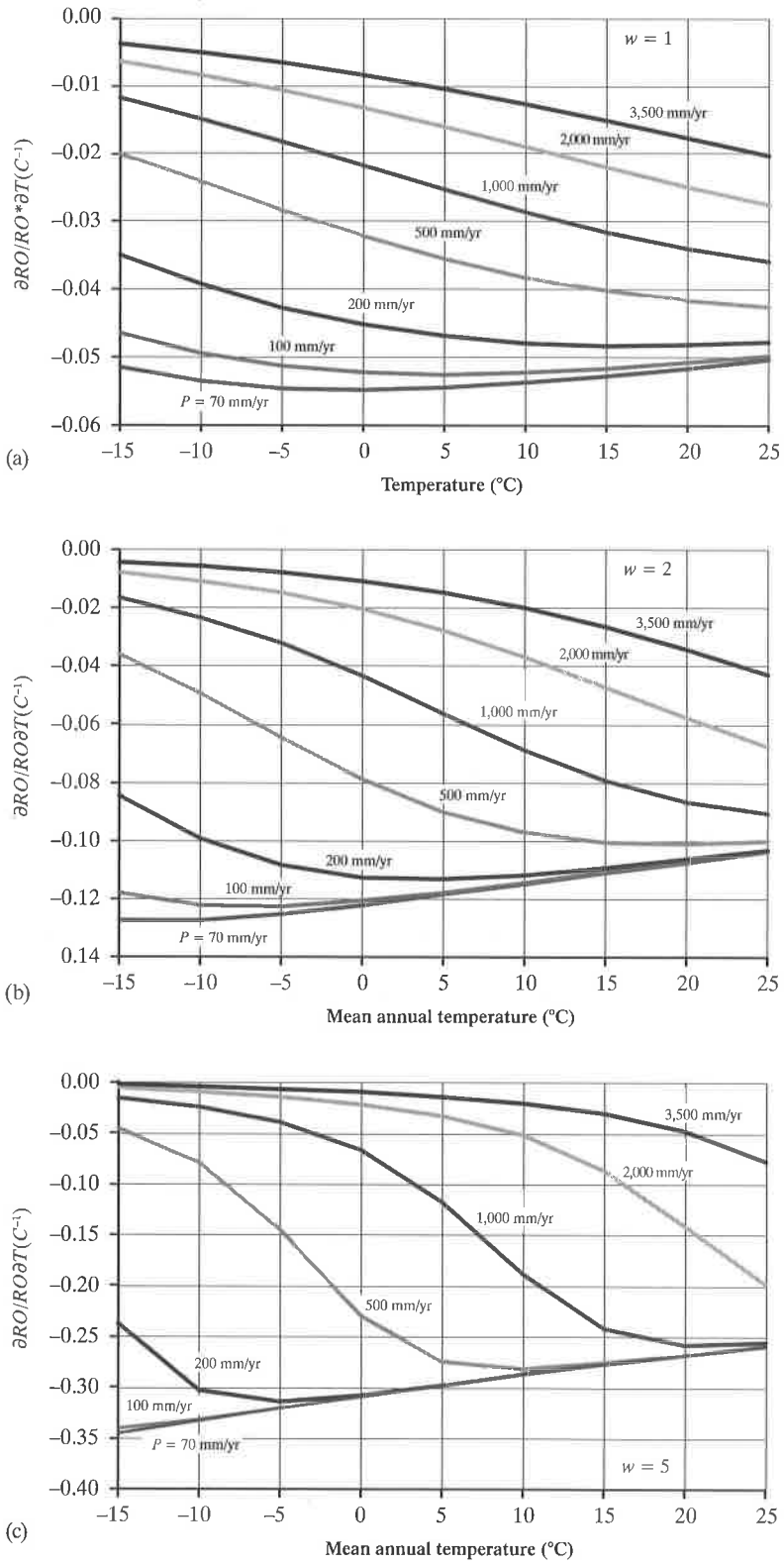

Figure 2.43 Relative change in average annual runoff ($\partial RO/RO$) per unit change in average annual temperature ($d\mathcal{T}$) as a function of annual average temperature ($\mathcal{T}$) as calculated in box 2.4. (a) $w = 1$; (b) $w = 2$; (c) $w = 5$.

$P(x,y)$ into two portions: one that has continental origin (i.e., most recently evaporated from any continental area), $P_C(x,y)$, and one that has an oceanic origin (i.e., most recently evaporated from the ocean), $P_O(x,y)$, and defined the local **precipitation-recycling ratio**, $R_P(x,y)$ as

$$R_P(x,y) \equiv \frac{P_C(x,y)}{P(x,y)} = \frac{P_C(x,y)}{P_C(x,y) + P_O(x,y)}. \quad \textbf{(2.17)}$$

$R_P(x,y)$ shows the dependence of precipitation at a given location (x,y) on upwind continental evapotranspiration to sustain precipitation. The local **evapotranspiration-recycling ratio**, $R_{ET}(x,y)$, was similarly defined as

$$R_{ET}(x,y) \equiv \frac{ET_C(x,y)}{ET(x,y)} = \frac{ET_C(x,y)}{ET_C(x,y) + ET_O(x,y)}, \quad \textbf{(2.18)}$$

where $ET_C(x,y)$ is terrestrial evapotranspiration that returns as continental precipitation, and $ET_O(x,y)$ is terrestrial evapotranspiration that precipitates on an ocean. Thus $R_{ET}(x,y)$ indicates the importance of evaporation at a certain location in sustaining downwind precipitation. Globally, the long-term average ET_C equals the average P_C.

Applying water-balance concepts (section 1.8) to the atmosphere, van der Ent et al. (2010) determined the global distribution of $R_P(x,y)$ (figure 2.44) and $R_{ET}(x,y)$ (figure 2.45). Oceanic sources are dominant in North America, though in the West about 60% of the evaporation returns to the continent downwind. South America shows three distinct moisture-recycling patterns: Evapotranspiration from the Guianas and the Amazon region becomes precipitation to the south in the Río de la Plata basin; there is local recycling east of the Andes; and there is very little moisture recycling in Patagonia. East Africa gets most of its precipitation from the Indian Ocean and, along with central Africa, contributes moisture to West Africa, which gets much of its precipitation from continental sources. Between Europe and Asia, the main moisture flux is westerly, as reflected in the eastward increase of $R_P(x,y)$; 40 to 70% of the evaporation from Europe returns to a continental area. Much of the precipitation in western and northern China, Mongolia, and Siberia is of continental origin. Local moisture recycling [high values of both $R_P(x,y)$ and $R_{ET}(x,y)$] is very important in the Tibetan plateau. Although most precipitation in the south of India, Southeast Asia, and Oceania is of oceanic origin, values of R_P near 30% indicate that continental precipitation is important there. In the northern part of Australia, Indonesia, and Papua New Guinea, which are very wet areas, $R_{ET}(x,y)$ is about 40%.

Table 2.13 summarizes the recycling ratios for the continents and gives the continental and global precipitation multipliers, $M_P(x,y)$, defined as

$$M_P(x,y) \equiv \frac{P(x,y)}{P_O(x,y)} = \frac{1}{1 - R_P(x,y)}. \quad \textbf{(2.19)}$$

$M_P(x,y)$ is the amplification of precipitation due to continental evaporation. When integrated over a

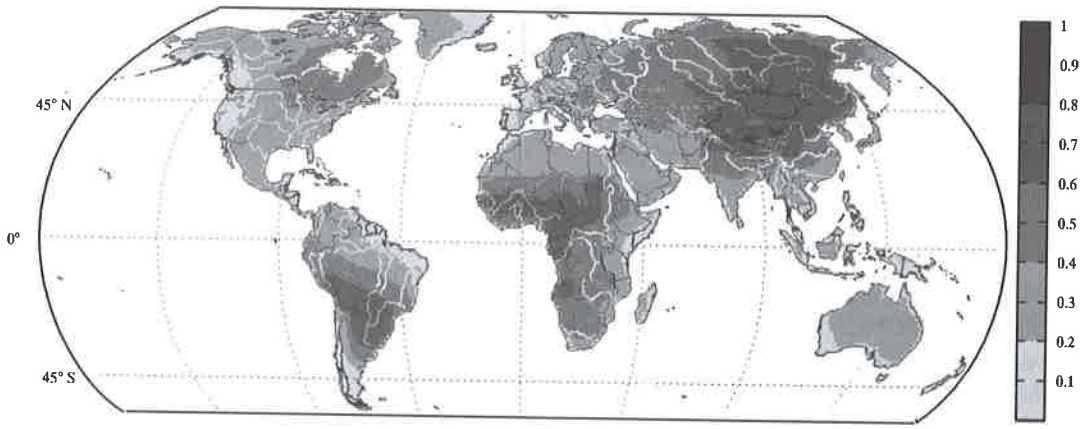

Figure 2.44 Average continental precipitation recycling ratio (1999–2008) [van der Ent et al. (2010). Origin and fate of atmospheric moisture over continents. *Water Resources Research* 46, with permission of the American Geophysical Union].

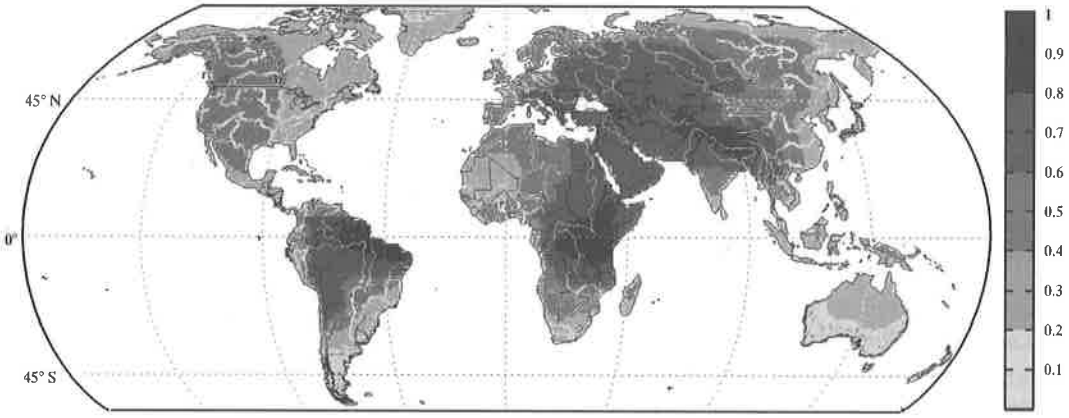

Figure 2.45 Average continental evapotranspiration recycling ratio (1999–2008) [van der Ent et al. (2010). Origin and fate of atmospheric moisture over continents. *Water Resources Research* 46, with permission of the American Geophysical Union].

year and all continental areas the multiplier is also the average number of times a water particle has sequentially fallen on the continent. As noted by van der Ent et al. (2010), recycled moisture multiplies precipitation by a factor 1.67 globally, and by much more in some regions: $M_P(x,y) = 3$ in the Río de la Plata basin in South America and is as high as 10 in western China.

Clearly, the feedbacks of moisture recycling play an important role in the global climate. Thus large-scale land-use changes currently taking place could interact with changes due to global warming, perhaps reinforcing them in some areas and weakening them in others. Clearly there is much to learn about the global hydrologic cycle and its complex feedbacks with human activities, and there are many potentially fruitful avenues of study. As noted by Eagleson (1986),

> Because of humanity's sheer numbers and its increasing capacity to affect large regions, the hydrologic cycle is being altered on a global scale with consequences for the human life support system that are often counterintuitive. There is a growing need to assess comprehensively our agricultural, urban, and industrial activities, and to generate a body of knowledge on which to base plans for the future. It seems safe to say that these actions must come ultimately from global-scale numerical models of the interactive physical, chemical, and biological systems of the earth. Of central importance among these systems is the global hydrologic cycle, and its representation in these models presents many analytical and observational challenges for hydrologists.

A major challenge for hydrologists is to establish the linkage between local-scale and global-scale processes, and this is the subject of much current re-

Table 2.13 Annual Average Moisture Recycling by Continent (1999–2008).

Region	Precipitation Recycling Ratio, R_P (%)	Evapotranspiration Recycling Ratio, R_{ET} (%)	Precipitation Amplification Factor, M_p
North America	27	35	1.37
South America	36	59	1.56
Africa	45	55	1.82
Europe	22	27	1.28
Asia	34	52	1.52
Oceania	18	27	1.22
All continents	40	57	1.67

Source: van der Ent (2010).

search. The final section of this chapter introduces some of the broad interconnections between soils and vegetation and hydrology. Subsequent chapters develop more detailed relations between soil and vegetation processes that control the land phase of the hydrologic cycle.

2.3 Hydrology and the Critical Zone

The **Critical Zone** (**CZ**) is "the heterogeneous, near surface environment in which complex interactions involving rock, soil, water, air and living organisms regulate the natural habitat and determine availability of life sustaining resources" (US National Research Council 2001).

The CZ extends from the top of the vegetation to the bottom of the aquifer (figure 2.46) and includes the near-surface biosphere and atmosphere, the pedosphere (the region in which soil-forming processes operate), and the surface and near-surface portions of the hydrosphere and lithosphere. Water movement is the principal agent in transporting mass and energy through the CZ. Because of the importance of these exchange processes to natural processes and to human life, there is increasing interest in focusing on the CZ as an integrating, although heterogeneous, framework for scientific study (Wilding and Lin 2006; Lin 2010).

Most of the following chapters of this book focus on the detailed processes of water movement and storage in the CZ. In the remainder of this chapter we introduce the broad relations between climate, hydrology, and the major CZ components, soils (the pedosphere), and vegetation (the biosphere).

2.3.1 Hydrology, Soils, and Climate

2.3.1.1 Soils and Hydrology

The conditions at the soil surface are a major determinant of hydrologic response to rain or snowmelt, as they determine whether water input moves downslope to streams quickly over the surface, or infiltrates to become subsurface runoff, water used in

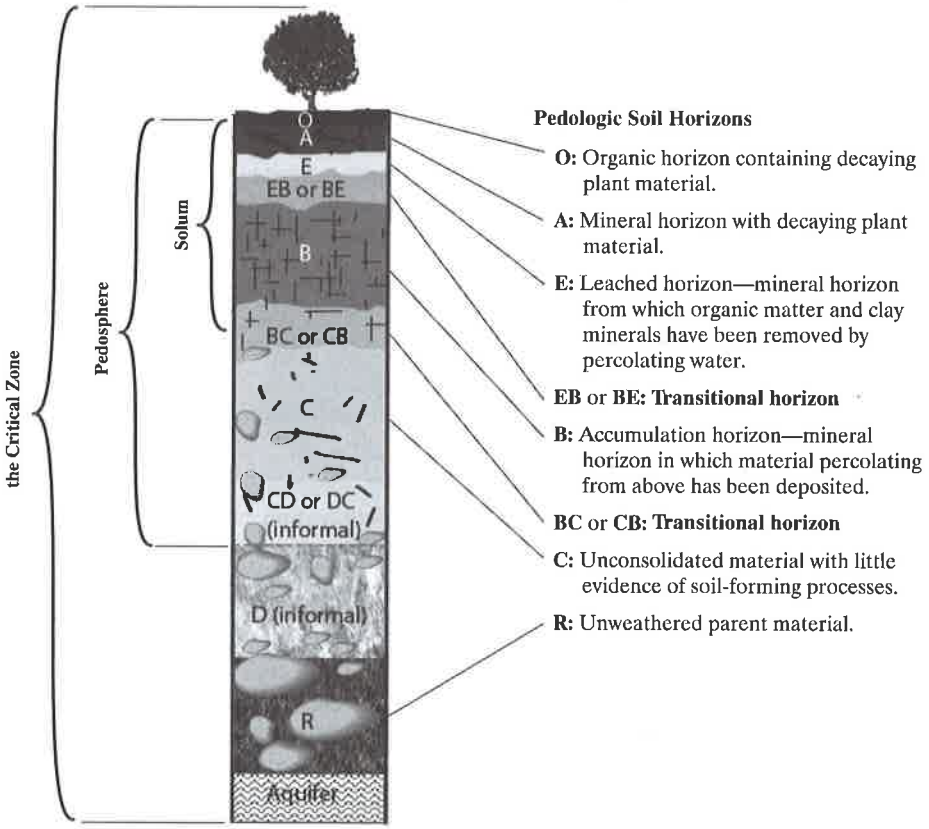

Figure 2.46
Components of the Critical Zone (CZ). The CZ extends from the top of the vegetation to the bottom of the aquifer and includes the near-surface biosphere and atmosphere, the pedosphere (the region in which soil-forming processes operate), and the surface and near-surface portions of the hydrosphere and lithosphere [adapted from Lin (2010)].